

Diffusion-Based Approximate MPC: Fast and Consistent Imitation of Multi-Modal Action Distributions

Pau Marquez Julbe[†], Julian Nubert^{†,*}, Henrik Hose[‡], Sebastian Trimpe[‡], and Katherine J. Kuchenbecker[†]

Abstract—Approximating model predictive control (MPC) using imitation learning (IL) allows for fast control without solving expensive optimization problems online. However, methods that use neural networks in a simple L2-regression setup fail to approximate multi-modal (set-valued) solution distributions caused by local optima found by the numerical solver or non-convex constraints, such as obstacles, significantly limiting the applicability of approximate MPC in practice. We solve this issue by using diffusion models to accurately represent the complete solution distribution (i.e., all modes) at high control rates (more than 1000 Hz). This work shows that diffusion-based AMPC significantly outperforms L2-regression-based approximate MPC for multi-modal action distributions. In contrast to most earlier work on IL, we also focus on running the diffusion-based controller at a higher rate and in joint space instead of end-effector space. Additionally, we propose the use of gradient guidance during the denoising process to consistently pick the same mode in closed loop to prevent switching between solutions. We propose using the cost and constraint satisfaction of the original MPC problem during parallel sampling of solutions from the diffusion model to pick a better mode online. We evaluate our method on the fast and accurate control of a 7-DoF robot manipulator both in simulation and on hardware deployed at 250 Hz, achieving a speedup of more than 70 times compared to solving the MPC problem online and also outperforming the numerical optimization (used for training) in success ratio. Project website: <https://paumarquez.github.io/diffusion-ampc>.

I. INTRODUCTION

Fast and dynamic systems are ubiquitous in robotics, ranging from autonomous vehicles to agile manipulation, where high-frequency control is essential for stability and precision. While diffusion models excel at high-level planning [1]–[3], low-level dynamic control tasks have not yet seen comparable advancements. This gap is particularly critical for systems requiring computationally efficient controllers that provide theoretical guarantees.

MPC is a versatile approach to control constrained linear and nonlinear systems [4]. By formulating a constrained optimization problem that is solved iteratively in closed loop, MPC provides stability guarantees, constraint satisfaction, and thus safety, and it has been successfully applied to a broad class of control problems. However, solving MPC optimization problems online remains a computational challenge in applications with fast dynamics, high update rates,

This work is funded in part by the Max Planck ETH CLS and the German Research Foundation (DFG): RTG 2236/2 (UnRAVeL).

[†]P. Marquez Julbe, J. Nubert, and K. J. Kuchenbecker are with the Max Planck Institute for Intelligent Systems, Stuttgart, Germany.

*J. Nubert is also with ETH Zürich, Switzerland.

[‡]H. Hose and S. Trimpe are with the Institute for Data Science in Mechanical Engineering (DSME), RWTH Aachen University, Germany.

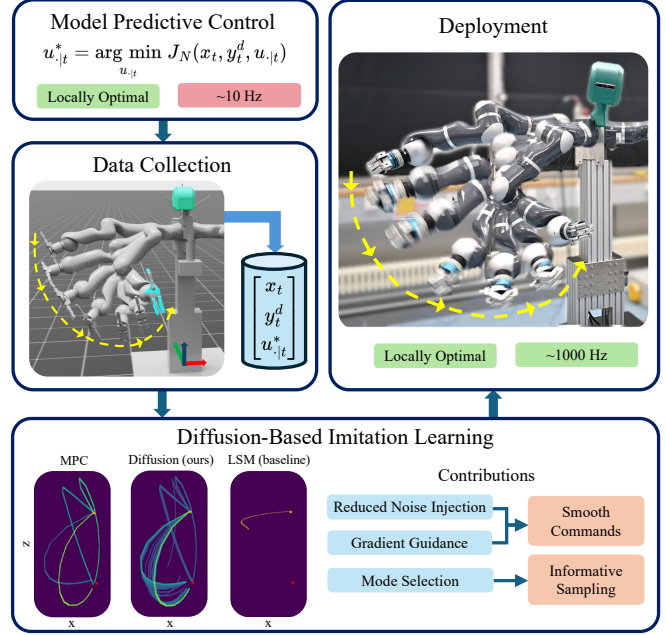


Fig. 1. The diffusion model uses IL to approximate the multi-modal action distribution of MPC optimization problems (lower left). We highlight advantages over classical AMPC and achieve high-quality solutions at fast update rates by *i*) stopping noise injection early, *ii*) using gradient guidance for closed-loop consistency, and *iii*) selecting the best mode online.

complex formulations like nonlinear or robust MPC, and deployment on resource-constrained embedded platforms. Several teams have bridged this gap with approximate MPC (AMPC), which bypasses online optimization by learning explicit controller representations through IL [5]. A common approach is to fit a multilayer perceptron (MLP) with least squares (LS) regression [6]–[11], which has shown promising results in practical settings [11]–[14]. Yet, one of the main issues experienced with AMPC based on a least squares model (LSM) is multi-modality in the mapping from state to expert trajectories [15]. When the MPC is formulated as a nonlinear and non-convex optimization problem, the solution is not guaranteed to be unique, as multiple or infinitely many local and/or global solutions can exist. Further, typical numerical solvers find only locally optimal solutions, which may lead to multi-modal (set-valued) distributions of a given state’s MPC control commands. Fundamentally, LS models cannot learn set-valued solutions [16] provided by the MPC expert and instead learn the non-optimal, and not necessarily feasible, mean of the conditioned target distribution.

In this work, we propose the use of diffusion models to approximate multi-modal solution distributions in AMPC

(Fig. 1). We can gracefully approximate inherently set-valued problems and local optima from numerical solvers. However, as shown in Sec. VI, naively sampling from the approximated solution distribution of the diffusion model leads to jerky and inconsistent robot behavior, as the policy output can alternate between different modes. We propose using gradient guidance (∇G) and early stopping (ES) of noise injection *during* denoising to achieve consistent and smooth action trajectories in closed loop. Further, *after* denoising we propose to *i*) check cost and constraint satisfaction of proposed solutions or *ii*) select the correct mode from the diffusion model through democratic voting. To evaluate our approach, we approximate a nonlinear MPC formulation for SE(3) setpoint tracking of a 7-degree-of-freedom (DOF) robotic manipulator in simulation and the real world including obstacle avoidance, commanding joint velocities from a given initial joint configuration. This task involves multiple local optima and set-valued global optima due to the non-convexity of the MPC and the robotic arm’s additional DOF. The proposed diffusion-based AMPC (DAMPC) significantly outperforms standard regression models in tasks with multiple solution modes. Interestingly, the diffusion model (DM) can even outperform the teacher MPC on some metrics.

Contributions: The contributions of this work are:

- 1) A novel diffusion-based AMPC formulation that captures multi-modal action distributions and significantly outperforms L2 regression.
- 2) A closed-loop AMPC framework capable of running at up to 1 kHz, including *i*) a denoising strategy to enhance closed-loop performance by improving consistency and smoothness (∇G and ES) and *ii*) parallel distribution sampling to either pick the best sample or perform majority voting.
- 3) First demonstration of diffusion-based AMPC on a real-world robotic system and comparison to LSM.

II. RELATED WORK

AMPC: Previous efforts in AMPC have focused on IL by collecting datasets of locally optimal MPC solutions and training a machine-learning model that predicts MPC control inputs. Many focus on machine-learning models trained with classic (L_2 -)regression [6,7,11,17,18]; also see [5] for a survey. While these models work for unimodal distributions, they cannot approximate the multi-modal distributions commonly found in non-convex MPC. Thus, multi-modal solutions must be avoided altogether in the dataset [15]. Multi-modal distributions in AMPC have already been approached using mixture density networks [19,20]. While these models are fast to evaluate, they require the number of modes as a hyperparameter of the model, which is difficult to know in practice. In contrast, diffusion can approximate arbitrary distributions in a single model.

DM: Previous investigations of diffusion models for robotics have primarily focused on higher-level planning by mapping RGB-D sensor data to expert actions from human demonstrations. Diffusers [2] use diffusion models to learn the dynamic model of a robotic arm and employ

guidance [21] to describe the task at hand by steering the sampling distribution to sample trajectories with desired initial and final states. Yet, [21] proposed to learn the joint distribution of state and action pairs, forcing the system to infer future states for every denoising step, adding computational overhead. In contrast, diffusion policy [1] is a diffusion model that learns the conditional distribution of the actions given the current observation; these authors performed real-time high-level end-effector position and velocity planning at 10 Hz in a receding horizon control fashion. Motion planning diffusion [3] learns a prior model over trajectories to perform robot navigation and injects gradient guidance for obstacle avoidance. Consistency policy [22] used consistency models to distill a diffusion policy to use fewer steps (between 1 and 3 denoising steps), allowing a much faster control rate. In this work, we propose a model that learns from MPC demonstrations while directly commanding joint-level actions. We use gradient guidance to achieve smooth trajectories without mode swaps.

Diffusion-based MPC: Recent works have used diffusion models to approximate an MPC formulation. Similar to our method, [23] and [24] propose imitation-learning approaches. The former finds globally optimal solutions similar to multi-start nonlinear solvers. However, the computational time of the approximation (more than 200 ms) is too large to control general dynamic robotic systems. The latter uses a diffusion model to learn trajectories of state-action pairs similarly to [2], and it generates safe trajectories with new constraints not present in the training dataset. Finally, [25] trains a DM using imitation learning and uses the approximation to warm-start an optimization solver. While they improve computational time, it remains unbounded with a high standard deviation, preventing this method from being deployed reliably in critical real-time systems. To our knowledge, we are the first to apply diffusion-based AMPC on real robotic hardware for low-level control at high update rates.

III. PROBLEM FORMULATION

We consider general, nonlinear, discrete-time systems $x_{t+1} = f(x_t, u_t)$, with state $x_t \in \mathcal{X} \subseteq \mathbb{R}^n$, input $u_t \in \mathcal{U} \subseteq \mathbb{R}^m$, time index $t \in \mathbb{N}$, and dynamics function $f : \mathcal{X} \times \mathcal{U} \rightarrow \mathcal{X}$. The control objective is to drive the system to a reference point where $h(x_t) = y_t^d$ and $f(x_t, u_t) = x_t$, where $y_t^d \in \mathcal{Y} \subseteq \mathbb{R}^n$ is the desired output and $h : \mathcal{X} \rightarrow \mathcal{Y}$ the output function.

A. Model Predictive Control in Simulation

We assume the existence of a general nonlinear MPC or trajectory optimization (TO) formulation that can solve the specified task under perfect assumptions in simulation:

$$\begin{aligned}
 u_{\cdot|t}^* &:= \arg \min_{u_{\cdot|t}, x_{\cdot|t}} J_N(u_{\cdot|t}; x_t, y_t^d) \\
 \text{s.t. } x_{0|t} &= x_t, \\
 x_{k+1|t} &= f(x_{k|t}, u_{k|t}), \\
 g_j(x_{k|t}, u_{k|t}) &\leq 0.
 \end{aligned} \tag{1}$$

Here, N is the prediction horizon with $k \in [0, 1, \dots, N-1] \in \mathbb{N}$, state $x_{\cdot|t} \in \mathcal{X}^N$, input $u_{\cdot|t} \in \mathcal{U}^N$, cost function

$J_N : \mathcal{U}^N \mapsto \mathbb{R}$, and constraints $g_j : \mathcal{X} \times \mathcal{U} \mapsto \mathbb{R}$ with p constraints. The feasible set \mathcal{Z} is defined as

$$\mathcal{Z} = \{(x, u) \in \mathcal{X} \times \mathcal{U} \mid g_j(x, u) \leq 0, j = 1, 2, \dots, p\}. \quad (2)$$

In simulation, an MPC controller solves Eq. (1) for each t and applies the policy $\pi_{\text{MPC}}(x_t) := u_{0|t}^*$ in closed loop.

B. Local Optimal Solver

We assume the availability of a local optimal solver of Eq. (1), denoted as s . In practice, s can be based on sequential quadratic programming, interior point methods, or even sampling-based zero-order methods. The corresponding solution depends on the initialization ξ^{init} of the optimization variables $\xi \in \Xi$ and parameters x_t and y^d . We do *not* assume to have an informed initial guess. The set of distributions of locally optimal solutions $u_{\cdot|t}^* := s(x_t, y^d, \xi^{\text{init}}) \in \mathcal{U}^N$ found by the solver s is given as

$$Q_s = \left\{ s(\xi^{\text{init}}, x_t, y^d) \mid \xi^{\text{init}} \sim \mathcal{P}(\Xi), x_t \in \mathcal{X}, y_t^d \in \mathcal{Y} \right\}, \quad (3)$$

where $\mathcal{P}(\Xi)$ denotes an arbitrary distribution over the optimization parameters Ξ .

C. Objective

We can sample from the set Q_s conditioned on x_t and y^d as $u_{\cdot|t}^* \sim Q_s(\cdot \mid x_t, y_t^d)$. Note that this policy is assumed to be non-deterministic, in contrast to most other AMPC formulations, e.g., [11]. This work aims to find an explicit approximation to reliably sample from Q_s at a fast update rate without numerically solving Eq. (1).

IV. METHOD: DIFFUSION-BASED APPROXIMATE MPC

This section describes the proposed DAMPC formulation of using a DM to sample from Eq. (3). The full system includes *data collection* (Sec. IV-A), DM prior *training* (Sec. IV-B), and DM *sampling* during inference (Sec. IV-C).

A. Data collection

We collect a dataset \mathcal{D} consisting of N_e episodes composed of the current state, desired setpoint, and locally optimal commands for N_d steps per episode. \mathcal{D} is given as $\mathcal{D} = \bigcup_{k=1}^{N_e} \mathcal{D}_k$ with each episode defined as

$$\mathcal{D}_k = \left\{ (kx_t, y_t^d, {}_k u_{\cdot|t}^*) \mid {}_k x_t \in \mathcal{X}, {}_k y_t^d \in \mathcal{Y}, u_{\cdot|t}^* \sim Q_s(\cdot \mid {}_k x_t, {}_k y_t^d), t = 1, \dots, N_d \right\}. \quad (4)$$

While storing optimal actions u^* , the generation of samples is performed by adding noise to the optimal MPC policy to reduce distribution shift [26] according to

$$\pi'_{\text{MPC}}(x_t) := \pi_{\text{MPC}}(x_t) + \sigma_{u_t} \epsilon, \quad \epsilon \sim \mathcal{N}(\mathbf{0}, \mathbf{I}), \quad (5)$$

with $\sigma_{u_t} := \max\left(\frac{|\pi_{\text{MPC}}(x_t)|}{\text{SNR}^d}, \sigma_{\min}\right)$ where SNR^d is the desired signal-to-noise ratio. Here, σ_{\min} is the minimum standard deviation of the noise added to explore regions of attraction near steady states. The policy π'_{MPC} is executed in simulation for N_d step episodes, N_e times. Unsatisfactory local minima are removed from the training dataset.

B. Diffusion-based MPC Prior Model

We train a diffusion model $f_\theta^{x_0}$ on the collected dataset \mathcal{D} to draw samples from the distribution $u_{\cdot|t}^* \sim Q_s(\cdot \mid x_t, y_t^d)$. We model the denoising process using Langevin dynamics and follow the standard Denoising Diffusion Probabilistic Model (DDPM) [27]. Here, a model $f_\theta^{x_0}(x_i, i)$ is trained to predict the clean sample x_0 from a given noisified sample x_i after i noisy steps in the *forward process*

$$q(x_i \mid x_{i-1}) := \mathcal{N}(x_i; \sqrt{1 - \beta_i} x_{i-1}, \beta_i \mathbf{I}), \quad (6)$$

where β_i is a parameter that adjusts the signal-to-noise ratio (SNR) at each step i depending on the chosen noise schedule. The training loss for $f_\theta^{x_0}$ can be derived and simplified from the variational bound on negative log likelihood (see [27] for details):

$$\mathcal{L}_{\text{ELBO}}^{x_0} := \|x_0 - f_\theta^{x_0}(\sqrt{\bar{\alpha}_i} x_0 + \sqrt{1 - \bar{\alpha}_i} \epsilon_i, i)\|^2. \quad (7)$$

C. Diffusion Model Sampling for Inference

Once $f_\theta^{x_0}$ is trained, samples from the underlying distribution of the training dataset can be drawn by gradually denoising an initial $x_{N_t} \in \mathcal{N}(\mathbf{0}, \mathbf{I})$ following

$$x_{i-1} := \frac{\sqrt{\bar{\alpha}_{i-1}} \beta_i}{1 - \bar{\alpha}_i} f_\theta^{x_0}(x_i, i) + \frac{\sqrt{\bar{\alpha}_i(1 - \bar{\alpha}_{i-1})}}{1 - \bar{\alpha}_i} x_i + \tilde{\beta}_i \epsilon, \quad (8)$$

where $\tilde{\beta}_i := \frac{1 - \bar{\alpha}_{i-1}}{1 - \bar{\alpha}_i} \beta_i$ and $\epsilon \sim \mathcal{N}(\mathbf{0}, \mathbf{I})$. This formulation is mathematically equivalent to predicting the added noise ϵ_i , instead of the clean sample x_0 . The mapping from predicted noise to clean sample is given by

$$x_0 = (x_i - \sqrt{1 - \bar{\alpha}_i} \epsilon) / \sqrt{\bar{\alpha}_i}, \quad (9)$$

which is relevant to exploit the diffusion model's relationship with score matching to allow for using ∇G [28]:

$$\nabla_x \log p(x) = -\frac{\epsilon}{\sqrt{1 - \bar{\alpha}_t}}. \quad (10)$$

In the following, we suggest three improvements on the denoising process during inference over DDPM [27].

1) *Consistent Mode Selection through Gradient Guidance*: In optimization-based real-time MPC, numerical solvers often show consistent mode selection in closed loop due to warm-starting. However, sampling from a diffusion model approximating multiple local solutions can lead to random mode selection in subsequent steps, causing inconsistent and jerky control commands. Inspired by warm-starting in real-time optimization, we propose to use *gradient guidance* for the DM to condition the distribution of the control commands to the previously executed command $p(u_t^* \mid x_t, y^d, u_{t-1}^*)$. Given a diffusion model that samples from Q_s , we transform $f_\theta^{x_0}$ into f_θ^ϵ by using Eq. (9) to exploit its relationship with score matching (Eq. (10)). Given $p(x_{i-1|t} \mid x_{i|t}, i)$ modeled by the DM [27], where i refers to the step during the denoising process, we can add prior information o by using Bayes' Rule [21]:

$$p(x_{i-1|t} \mid x_{i|t}, i, o) \propto p(x_{i-1|t} \mid x_{i|t}, i) p(o \mid x_{i|t}, i). \quad (11)$$

By using the log's property, this can be written as

$$\begin{aligned} \nabla_x \log p(x_{i-1|t}|x_{i|t}, i, o) &\propto \nabla_x \log p(x_{i-1|t}|x_{i|t}, i) \\ &+ \nabla_x \log p(o|x_{i|t}, i). \end{aligned} \quad (12)$$

Therefore, we can guide the distribution toward the previous mode to ensure closed-loop consistency by redefining f_θ^ϵ as

$$\begin{aligned} f_\theta^\epsilon(x_{i|t}, i, o) &:= f_\theta^\epsilon(x_{i|t}, i) - \\ &\nabla_{x_{i|t}} \log \mathcal{N}(x_{i|t}; x_{0|t-1}, (1 - \bar{\alpha}_i)\mathbf{I}). \end{aligned} \quad (13)$$

2) Reduced Jerk by Stopping Noise Injection Early:

During denoising, randomness is added via the noise schedule $\tilde{\beta}_i$ in Eq. (8), balancing smoothness and sample diversity. For high-frequency control, smooth solutions are prioritized over exploration to prevent vibrations. Thus, we propose to perform denoising as

$$x_{i-1} := \frac{\sqrt{\bar{\alpha}_{i-1}}\beta_i}{1 - \bar{\alpha}_i}x_0 + \frac{\sqrt{\bar{\alpha}_i}(1 - \bar{\alpha}_{i-1})}{1 - \bar{\alpha}_i}x_i + \tilde{\beta}_i\epsilon, \quad (14)$$

where $\tilde{\beta}_i := \tilde{\beta}_i \mathbf{1}_{i > i_{\min}^\epsilon}$ and $\epsilon \sim \mathcal{N}(\mathbf{0}, \mathbf{I})$. Adding noise at the lower SNR steps allows the diffusion model to explore multi-modality. Not adding the noise at the higher SNR steps allows the closed-loop function to be smooth, considerably reducing the resulting trajectory's jerk.

3) Constraint Satisfaction via Sampling in Closed Loop:

We propose methods for informative sampling from $Q_s(\cdot | x_t, y_t^d)$ to reduce approximation uncertainty and improve sample fidelity. Similar to multi-start methods [23] for non-linear optimization, we generate L inputs $\{u_i^* | u_i^* \sim Q_s(\cdot | x, y^d)\}_{i=1}^L$ by sampling the diffusion model (leveraging GPU parallelization) and suggest *two* ways to rank these samples.

a) Full State Knowledge Available: We can score and rank the samples according to these criteria when checking feasibility and (MPC) cost online.

b) No Full State Knowledge: When we cannot reliably estimate the cost of each sample, e.g., when the diffusion model is implicitly estimating the state of the system, we propose clustering the samples based on a similarity metric, such as the Euclidean distance in the command space, or a domain-specific distance measure. Let $\mathcal{C} = \{C_1, C_2, \dots, C_K\}$ represent K clusters, where each cluster C_k corresponds to a distinct mode of the distribution. The probability mass of each cluster is approximated by the empirical density $P(C_k) \approx \frac{|C_k|}{L}$. The selected trajectory u_i^* is drawn from the highest-density cluster, ensuring that the chosen trajectory is representative of the most probable mode in the distribution, discarding low-density samples that commonly correspond to unsuccessfully denoised samples or unlikely local minima generated by the MPC during data collection.

V. SETUP & IMPLEMENTATION DETAILS

To assess the performance of our method, we approximate an MPC formulation for full SE(3) end-effector tracking of a 7-DOF *KUKA LBR4+* arm (Fig. 1) by commanding joint velocities at a high rate. This task exposes multi-modality due to the redundant DOF, obstacles in the environment, and the implicit non-convexity of the optimization problem. In this section, we explain the MPC formulation and the design parameters of the data collection, baselines, and DAMPC.

A. Model Predictive Control for End-Effector Pose Tracking

We use an MPC formulation based on [11,29,30] extended to track full SE(3) end-effector poses. We define a state $x_t \in \mathcal{X} \subset \mathbb{R}^7$ as the joint positions and $u_t \in \mathcal{U} \subset \mathbb{R}^7$ as the joint velocities. As opposed to [11], and following [30, Ass. 1], we define a virtual trajectory $x_{\cdot|t}^s \in \mathcal{X}^{N+1}$ and input $u_{\cdot|t}^s \in \mathcal{U}^{N+1}$, with a reference $y_t \in \text{SE}(3) = \mathcal{Y}$ and virtual output $y^s = h(x_{N|t}^s)$. The control objective is the minimization of the tracking error $e_t = x_{N|t}^s - x_t$ and constraint satisfaction $(x_t, u_t) \in \mathcal{Z}$. We found that a virtual trajectory instead of a virtual terminal state as in [11] improved convergence. The corresponding MPC formulation for output tracking is:

$$\begin{aligned} \min_{u_{\cdot|t}, u_{\cdot|t}^s, x_{\cdot|t}^s} & J_N(u_{\cdot|t}, u_{\cdot|t}^s, x_{\cdot|t}^s; x_t, y_t^d) \\ \text{s.t. } & x_{0|t} = x_t, \quad x_{0|t}^s = x_t \\ & x_{k+1|t} = f(x_{k|t}, u_{k|t}), \quad x_{k+1|t}^s = f(x_{k|t}^s, u_{k|t}^s), \\ & g_j(x_{k|t}, u_{k|t}) \leq 0, \quad g_j(x_{k|t}^s, u_{k|t}^s) \leq 0, \\ & f(x_{N|t}^s, u_{N|t}^s) = x_{N|t}^s, \end{aligned} \quad (15)$$

for $k = 0, 1, \dots, N-1$, where the cost is

$$\begin{aligned} J_N(u_{\cdot|t}, u_{\cdot|t}^s; x_t, y_t^d) &:= \left\| x_{N|t} - x_{N|t}^s \right\|_{\mathbf{P}} + \\ & d_y(y_t^d, h(x_{N|t}^s)) + \sum_{k=0}^{N-1} l(x_{k|t}, u_{k|t}, x_{k|t}^s, u_{k|t}^s), \end{aligned} \quad (16)$$

with quadratic stage cost $l(x, u, x^d, u^d) = \|x - x^d\|_{\mathbf{Q}}^2 + \|u - u^d\|_{\mathbf{R}}^2$ with positive definite \mathbf{Q} and \mathbf{R} . The dynamics function f is the Euler integration of the joint position $x_{k|t}$ with the joint velocity commands $u_{k|t}$. The output error $d_y : \text{SE}(3) \times \text{SE}(3) \mapsto \mathbb{R}$ is given by a weighted average of the position distance $\|y_p - h(x^s)_p\|_2^2$ and the rotation distance $\|(\log(y_R^{-1}h(x^s)_R))_{\vee}\|_2^2$, where the subindex p and R denote the position and rotation components of SE(3) elements. Furthermore, $\log(\cdot)$ refers to the mapping from the Lie group SE(3) to the Lie algebra $\mathfrak{se}(3)$, and $[\cdot]_{\vee}$ is the projection from the Lie algebra to the tangent space. The constraint set \mathcal{Z} is defined with polytopic constraints on the state and command limits, and spherical obstacle avoidance constraints

$$\|(h(x_{k|t}^i)_p - o_j^p) \odot o_j^s\|_2 \geq 1 \quad (17)$$

on the output space \forall time steps $k \in [0, \dots, N-1] \subset \mathbb{N}$, joints $i \in [1, \dots, 7] \subset \mathbb{N}$, and obstacles $j \in [1, \dots, M] \subset \mathbb{N}$ with M obstacles. The ellipsoidal regions representing the robot's body and external objects are defined by position $o_j^p \in \mathbb{R}^3$ and scaling $o_j^s \in \mathbb{R}^3$. The \odot refers to the element-wise product.

B. Data Collection

We collect two datasets: the first has only self-collision avoidance, and the second adds a spherical obstacle in the center of the task space to assess non-convex constraint satisfaction of the approximation. We collect the datasets with the method explained in Sec. IV-A for $N_d = 80$ step episodes with random initial joint positions $x_0 \in \text{Unif}(\mathcal{X})$ and reachable targets $y^d \in \text{Unif}(\mathcal{Y}^d)$ where $\mathcal{Y}^d := \{h(x) | x \in$

\mathcal{X} . The final datasets contain 55.5 and 33.9 million open-loop MPC predictions, respectively. The prediction horizon is $N = 20$ and $\Delta t = 0.1$ s. The state constraints are given by the joint limits, and the input constraints by the *KUKA*'s safety stop, which engages beyond $2.3 \frac{\text{rad}}{\text{s}}$. The noise coefficients for exploration are $\text{SNR}^d = 0.8$ and $\sigma_{\min} = 0.35 \frac{\text{rad}}{\text{s}}$. These values were chosen empirically by increasing noise to the maximum level that allows the target to be reached. We use IPOPT [31] as solver s and uniformly randomize the initial guess ξ_{guess} at $t = 0$. For subsequent steps, we warm-start the solver with the previous solution to ensure mode diversity in the dataset. We excluded unsatisfactory solutions where $d_y(y_t^d, h(x_{N|t}^s)) > 0.01$, which we attribute to the random initial guess, thereby removing 5% of the dataset.

C. Implementation Details

The data collection pipeline is built on top of Isaac Lab [32] with expert solutions computed with IPOPT [31] on CPU using CasADi [33] and Pinocchio [34]. Using multi-processing techniques, we deploy CoClusterBridge to parallelize the data collection on the vectorized simulator. For each dataset we train a DM and a nonlinear LSM as a baseline. The observations of the models are the current joint state x_t and the position and orientation of the target y^d , where the orientation is encoded with the 6D representation provided by [35]. The diffusion model is trained based on DDPM [27] using a cosine noise scheduler [36] for 5 steps with the rescaling proposed by [37] to ensure 0 SNR at the last step. We use the default $\gamma = 5$ for the Min-SNR weighting strategy [38]. For inference we use the proposed ∇G (Sec. IV-C.1) to ensure consistency within subsequent closed-loop steps, and we set $i_{\min}^\epsilon = \lfloor 0.75 \cdot N_I \rfloor$ from Eq. (8) and Eq. (14) to perform early stopping, where N_I is the total number of denoising steps. The model architecture is an MLP composed of 7 layers with 1,000 neurons each, with a total of 6.6 million trainable parameters (note that we did not optimize to reduce the size of this network), as well as MLPs for the temporal and observation encoder. The baseline LS model has 6 layers and a total of 2.8 million trainable parameters, tuned to minimize the validation loss.

D. Hardware Deployment

We deploy the LSM and the proposed DAMPC controller with ∇G and ES on a *KUKA LBR4+* robotic arm (Apollo, [39]) at a control rate of 250 Hz. We also compare to the optimization-based MPC, which is limited to 10 Hz due to slow execution. The policies run on an *Intel Core i9-13900K* and an *NVIDIA GeForce RTX 4070*; low-level PI controllers track the commanded joint velocities at 1 kHz.

VI. RESULTS

We evaluate the performance of the proposed diffusion-based approximation both in a kinematic simulation and on hardware experiments using Apollo. First, we evaluate the proposed denoising strategies of Sec. IV-C.1 and Sec. IV-C.2, showing why the proposed variations of standard DDPM are

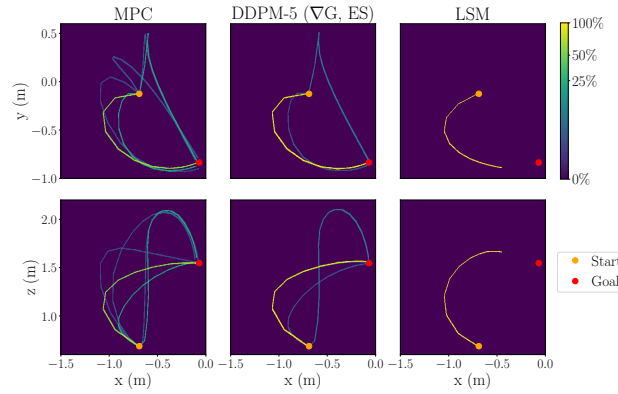


Fig. 2. Heatmaps representing the end-effector position’s probability density (log scale), projected onto the x - y and x - z planes over multiple runs for the same start x_0 and goal y^d . Qualitative multi-modality of (open-loop) MPC solutions $x_{\cdot|0}$ are shown on the left, which are approximated well by DDPM (ours, center). In contrast, the LSM (right) collapses to the dominant mode without reaching the target.

needed for hardware deployment. Then, we analyze the informative sampling strategies from Sec. IV-C.3 by leveraging the model’s ability to provide a large set of samples.

A. Denoising Methods for Diffusion-based Control

This section provides results for DDPM with ∇G and ES (ours), as well as the following baselines: vanilla DDPM [27], Denoising Diffusion Implicit Model (DDIM) [40] to reduce denoising steps during inference, and LSM (MLP with L2-regression loss). We quantitatively and/or qualitatively report each method’s ability to represent multi-modal action distributions (Sec. VI-A.1), tracking performance (Sec. VI-A.2), the effectiveness of ∇G and ES (Sec. VI-A.3), feasibility (Sec. VI-A.4), and computational time (Sec. VI-A.5) via simulation and hardware experiments.

1) *Representing Multi-Modality:* We verify approximation of the multi-modal distributions qualitatively in simulation. As shown in Fig. 1 and Fig. 2 (left), the solution to the MPC optimization is a multi-modal distribution of open-loop end-effector trajectories (i.e., the predicted $x_{\cdot|0}$ from Eq. (15)) for different initial guesses ξ but the same initial state x_0 and desired output y^d . Indeed, the LSM cannot approximate multi-modal distributions, as shown in Fig. 2 (right). However, when one trajectory dominates the density, the LSM can decently predict this primary mode. The proposed DM can capture multiple different modes and predict long-horizon trajectories (center of Fig. 2). Notably, some modes of the MPC solution distribution are not reproduced by the diffusion model because we filter out local minima that do not reach the target (cf. Sec. V-A) and because the model has only 5 denoising steps. Models trained with more denoising steps, e.g., 40, generally capture low-density modes more completely.

2) *Tracking Performance:* We quantitatively evaluate tracking performance for 8,750 random start and goal poses in simulation and 100 in hardware experiments. The success rates (SRs), defined as the proportion of trajectories that terminate with errors below 20 mm and 5.7° , the transient response times (TRTs), absolute translation errors (ATEs),

TABLE I. Closed-loop tracking performance in **non-real-time** simulation for random start and goal positions. Mean ATE, ARE and TRT are computed only for successful episodes, the rate of which we report under SR. The proposed approach is shown in **blue**.

Method	N_I	∇G	ES	ATE [mm]	ARE [$^\circ$]	SR [%]	TRT [s]
MPC				0.54	0.02	93.18	1.18
LSM				13.84	3.70	10.26	2.54
DDPM	5	×	×	5.63	1.29	95.76	1.14
DDPM	5	×		5.63	1.29	95.71	1.14
DDPM	40			5.14	1.21	96.18	1.18
DDPM	5			5.47	1.26	96.33	1.17
DDIM	5			5.07	1.19	96.41	1.18

TABLE II. Closed-loop **hardware** experiments for random start and goal positions. Mean ATE, ARE and TRT are computed for successful episodes, which occur at the rate of SR. DDPM without guidance is *not deployable* due to mode swapping in subsequent closed-loop steps, which leads to high jerk and unsafe behavior. The proposed approach is shown in **blue**.

Method	N_I	∇G	ES	ATE [mm]	ARE [$^\circ$]	SR [%]	TRT [s]
MPC				3.71	0.40	87.80	1.71
LSM				15.77	3.94	12.90	2.62
DDPM	5	×	×	6.16	1.29	93.00	1.34

and absolute rotation errors (AREs) thereof are reported in Tab. I for simulation and Tab. II for hardware experiments. The SR of the proposed method is higher than that of the optimization-based MPC in both settings due to convergence issues that appear only occasionally. Removing these from the training dataset allows our DM to outperform the expert in SR. Regarding translation and orientation error at the end of successful runs, the MPC achieves the best metrics in simulation and hardware, reaching 0.5mm error during the 5s episode in the perfect simulations. In contrast, the diffusion-based approximators achieve a steady-state error of about 5mm, likely due to the emphasis of the data collection process on dynamic regions and the added noise $\sigma_{\min} \gg 0$. The LSM shows poor tracking quality and rarely converges as it fails to approximate multi-modal behavior.

For the simulation results in Tab. I, we additionally report the performance of vanilla DDPM with 40 and 5 denoising steps, and vanilla DDIM with 5 denoising steps. While all of these show similar steady-state performance in simulation, we *cannot* evaluate these controllers on hardware due to vibrations and jerky behavior caused by inconsistent mode selection (without ∇G), as detailed in the following section.

We also report the evolution of the average tracking error over time for closed-loop experiments on hardware in Fig. 3. The MPC has poor transient performance and high overshoot, potentially leading to self-collisions, due to its slow update rate of 10 Hz. In comparison, the transient performance of the proposed diffusion model and the LSM benefit from the approximation’s fast 250 Hz update rate; they show smooth behavior with little or no overshoot. The LSM has large overall tracking error due to multi-modality.

3) *Gradient Guidance and Early Stopped Noise Injection:* We evaluate the effectiveness of *i)* using ∇G to remove mode swapping and *ii)* reducing the noise level for later denoising steps, compared to vanilla DDPM and DDIM. To this end, we compare the number of mode changes in closed loop to showcase the effectiveness of guidance and

TABLE III. ∇G and ES noise injection in simulation. Mode swaps are defined as the number of different local minima chosen. Statistics are extracted from episodes of 2s. The median jerk norm shows the effectiveness of the noise schedule. The proposed method is shown in **blue**.

Method	N_I	∇G	ES	Mean Mode Swaps per Episode [%]	Median Jerk Norm [rads $^{-3}$]
MPC				0.15	8.00
LSM				0.00	88.60
DDPM	5	×	×	0.01	57.76
DDPM	5	×		0.08	2403.78
DDPM	40			3.78	354.84
DDPM	5			3.00	1149.10
DDIM	5			3.93	1267.84

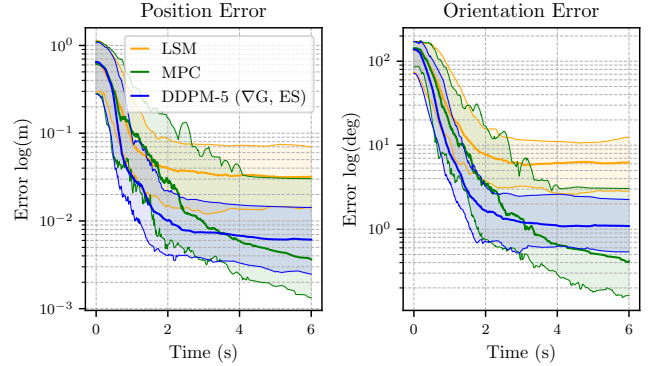


Fig. 3. Tracking performance in closed-loop hardware experiments: mean end-effector position and orientation errors over time for the LSM, the optimization-based MPC, and the proposed diffusion model with five denoising steps, gradient guidance, and early stopped noise injection. The shaded areas show the 10th to 90th error percentiles.

the median jerk to assess the effect of the noise schedule. An exemplary trajectory is visualized in Fig. 4, and quantitative metrics are reported in Tab. III. Quantitatively, guidance significantly reduces mode swaps compared to vanilla diffusion and even MPC with optimization, which underlines the effectiveness of our contribution. While guidance shows significant jerk, early stopped noise injection reduces this by orders of magnitude and achieves smooth control with only 5 denoising steps. In Fig. 4, vanilla DDPM and DDIM with 5 denoising steps exhibit interleaved modes. Adding guidance provides consistency across the entire episode. In addition, the noise schedule removes remaining jerkiness of the commands. Notably, only policies with guidance could be deployed on hardware.

4) *Feasibility Analysis:* Thus far, tracking performance, mode consistency, and smoothness have been of significant concern. In this section, we analyze constraint satisfaction in the presence of non-convex constraints, in particular due to a spherical obstacle in the task space. Fig. 5 shows the *cumulative distribution of the obstacle penetration*. The LSM cannot model the non-convex constraint, thus showing poor constraint satisfaction. DDPM with 5 and 40 denoising steps show similar distributions in open and closed loop, with high density near the 0% penetration (surface), demonstrating once more the advantage over LSM and suggesting that five denoising steps suffice for this approximate MPC application.

5) *Computational Time:* Tab. IV shows the computational time of our approach and MPC implementation. We achieved a $5.6\times$ speed-up on the CPU and a $73\times$ speed-up on the GPU.

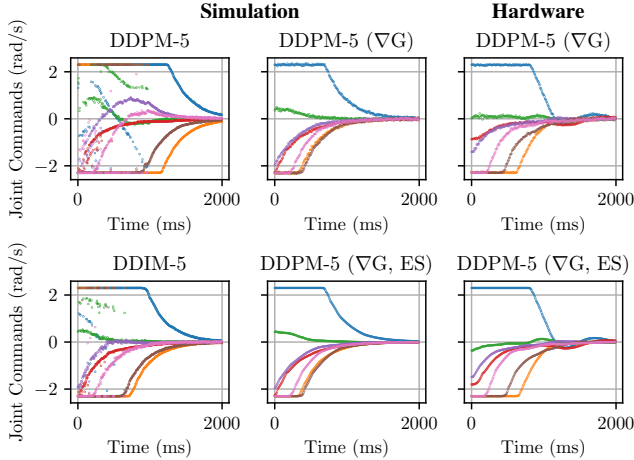


Fig. 4. Exemplary closed-loop joint commands of vanilla diffusion models in simulation (left), the DDPM with gradient guidance (∇G) in simulation (center top) and hardware (right top), the proposed DDPM with five steps, ∇G , and early stopping (ES) in simulation (center bottom) and hardware (right bottom). ∇G ensures consistent modes necessary for hardware deployment, while ES smooths the commands.

B. Sampling from Diffusion Models

So far, we have evaluated the quality of individually sampled trajectories using the DM. In this section, we inspect how drawing a larger batch of samples from the DM’s distribution can boost performance by selecting the trajectory with lowest MPC cost, selecting only feasible trajectories, or through democratic voting. Informative sampling reduces uncertainty and generally avoids selecting low-density modes that are either unsuccessfully denoised samples (e.g., caused by a low number of denoising steps) or low-density modes in the expert distribution that can be considered artifacts but were not removed from the dataset.

1) *Tracking Performance*: Tab. V shows how leveraging different sampling techniques improves SR and TRT without hindering steady-state performance. Using the MPC cost to select the optimal mode provides the best results, at a computational expense dependent on the application. Clustering improves standard sampling without environment knowledge.

TABLE IV. Computational time of the proposed method compared to the MPC and DDPM with 40 denoising steps on the CPU or GPU.

Method	N_I	∇G	ES	Mean [ms]		Perc 95th [ms]	
				CPU	GPU	CPU	GPU
MPC				47.54	-	65.63	-
DDPM	5	×	×	9.77	0.85	11.57	0.90
DDPM	40	×	×	107.18	3.79	112.76	3.81

TABLE V. Closed-loop tracking performance in **non-real-time** simulation for random start and goal positions. Mean ATE, ARE and TRT are computed only for successful episodes, the rate of which we report under SR. All diffusion models are deployed using ∇G and ES.

Method	Sampling	ATE [mm]	ARE [°]	SR [%]	TRT [s]
MPC		0.54	0.02	93.18	1.18
LSM		13.84	3.70	10.26	2.54
DDPM	-	5.63	1.29	95.76	1.14
DDPM	Cluster	5.61	1.29	96.09	1.13
DDPM	Cost	5.66	1.31	97.51	1.09

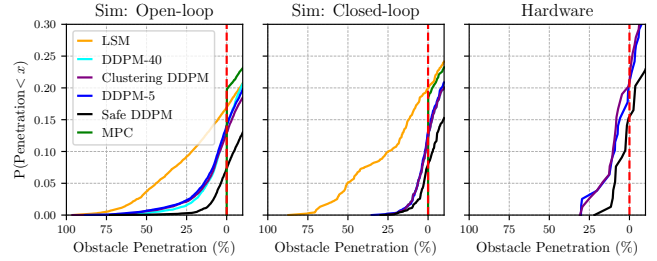


Fig. 5. Constraint satisfaction of open-loop predicted action sequences (left), the resulting closed-loop trajectories in simulation (center), and closed-loop experiments on hardware (right). The graphs show the cumulative distribution of the penetration error of a spherical obstacle relative to its 20 cm radius. All DMs are evaluated with ∇G and ES.

2) *Feasibility Analysis*: Tab. VI shows feasibility metrics for sampling strategies in simulation and hardware experiments. Clustering slightly improves performance in simulation. However, hardware experiments are inconclusive due to the similar performance with and without clustering. DDPM-Safe samples 100 trajectories with guidance and randomly picks one from the non-colliding subset, showing a clear improvement over standard DDPM. To avoid jerky motions, we have applied guidance to both sampling methods, thereby narrowing multi-modality for sampling strategies in closed loop and somewhat hindering performance.

3) *Computational Time*: Tab. VII shows sampling method costs. Modern GPUs can perform batched computations with negligible overhead, leading to only a slight increase in computational time with respect to naive sampling (see Tab. IV), even with a batch size of 100. On CPU, a batch of 100 leads to a $4\times$ increase in computational time, which is satisfactory for specific embedded applications.

VII. CONCLUSIONS & FUTURE WORK

We proposed DAMPC, a diffusion-based AMPC formulation capable of capturing multi-modal action distributions from a nonlinear MPC demonstrator. By introducing specific design choices and reducing the number of denoising steps, we showed that diffusion models can be used for fast (>100 Hz) and accurate control on real robotic systems, allowing for a speedup of more than $70\times$ compared to the optimization-based MPC. By controlling a 7-DOF manipulator that exhibits multi-modal action distributions, we showed that consistent mode selection and reducing jerk in actions are essential for successful hardware deployment, which we achieved during the denoising process using ∇G and ES.

TABLE VI. Constraint satisfaction in closed-loop simulation and hardware in terms of SR for 10% and 1% tolerance. Sampling multiple action sequences and choosing a safe one improves constraint satisfaction compared to naive sampling. The baseline LSM performs poorly with non-convex constraints. The proposed approach is shown in blue.

Method	Sampling	Simulation		Hardware	
		10% SR	1%SR	10% SR	1%SR
MPC		100.00	100.00	-	-
LSM		84.20	80.30	81.25	75.00
DDPM	-	97.40	88.50	90.00	81.25
DDPM	Cluster	97.70	88.90	88.75	80.00
DDPM	Safe	99.20	95.10	95.00	85.00

TABLE VII. Computational time of the proposed sampling methods for CPU and GPU with a sample size of 100, 5 denoising steps, ∇G , and ES. The computational time increase is small compared to Tab. IV due to parallelization (particularly on GPU). The cost sampling runs on the CPU.

Method	Sampling	Mean [ms]		Perc 95th [ms]	
		CPU	GPU	CPU	GPU
DDPM	Cluster	23.602	1.345	36.870	1.391
DDPM	Safe	28.380	3.305	45.548	3.525
DDPM	Cost	27.539	4.499	44.765	4.625

For future work, we plan to expand our results to higher-dimensional input and state spaces, e.g., vision, to utilize the potential of diffusion models fully. Moreover, in the current setup, the required training data remains high, resulting in slow synthesis of policies. A more-efficient sampling strategy during data generation could help generate new policies more efficiently. Applying DAMPC to embedded hardware by downsizing the MLP or applying quantization and pruning could further open up new application domains.

ACKNOWLEDGMENTS

We thank F. Grimminger, V. Berenz, B. Javot, and O. B. Aladag for supporting our experiments with the Apollo robot.

REFERENCES

- [1] C. Chi, S. Feng, Y. Du, Z. Xu, E. Cousineau, B. Burchfiel, and S. Song, "Diffusion policy: Visuomotor policy learning via action diffusion," in *Robotics: Science and Systems (RSS)*, 2023.
- [2] M. Janner, Y. Du, J. Tenenbaum, and S. Levine, "Planning with diffusion for flexible behavior synthesis," in *Proc. the Int. Conf. on Machine Learning (ICML)*. PMLR, 2022.
- [3] J. Carvalho, A. T. Le, M. Baiert, D. Koert, and J. Peters, "Motion planning diffusion: Learning and planning of robot motions with diffusion models," in *Proc. IEEE/RSJ Int. Conf. on Intelligent Robots and Systems (IROS)*, 2023.
- [4] J. Rawlings, D. Mayne, and M. Diehl, *Model Predictive Control: Theory, Computation, and Design*, 2017.
- [5] C. Gonzalez, H. Asadi, L. Kooijman, and C. P. Lim, "Neural networks for fast optimisation in model predictive control: A review," *arXiv:2309.02668*, 2023.
- [6] H. Hose, J. Köhler, M. N. Zeilinger, and S. Trimpe, "Approximate non-linear model predictive control with safety-augmented neural networks," *arXiv preprint arXiv:2304.09575*, 2023.
- [7] T. Parisini and R. Zoppoli, "A receding-horizon regulator for nonlinear systems and a neural approximation," *Automatica*, 1995.
- [8] S. Lucia and B. Karg, "A deep learning-based approach to robust nonlinear model predictive control," in *Proc. IFAC Conference on Nonlinear Model Predictive Control (NMPC)*, vol. 51, no. 20, 2018.
- [9] A. D. Bonzanini, J. A. Paulson, G. Makrygiorgos, and A. Mesbah, "Fast approximate learning-based multistage nonlinear model predictive control using Gaussian processes and deep neural networks," *Computers & Chemical Engineering*, vol. 145, p. 107174, 2021.
- [10] J. Drgoňa, K. Kis, A. Tuor, D. Vrabie, and M. Klauco, "Differentiable predictive control: Deep learning alternative to explicit model predictive control for unknown nonlinear systems," *Journal of Process Control*, vol. 116, pp. 80–92, 08 2022.
- [11] J. Nubert, J. Köhler, V. Berenz, F. Allgöwer, and S. Trimpe, "Safe and fast tracking on a robot manipulator: Robust mpc and neural network control," *IEEE Robotics and Automation Letters*, vol. 5, no. 2, 2020.
- [12] M. Abu-Ali, F. Berkel, M. Manderla, S. Reimann, R. Kennel, and M. Abdelrahem, "Deep learning-based long-horizon MPC: Robust, high performing, and computationally efficient control for pmsm drives," *IEEE Trans. on Power Electronics*, vol. 37, no. 10, 2022.
- [13] H. Hose, A. Gräfe, and S. Trimpe, "Parameter-adaptive approximate MPC: Tuning neural-network controllers without retraining," in *Learning for Dynamics and Control Conference*. PMLR, 2024.
- [14] H. Hose, J. Weisgerber, and S. Trimpe, "The Mini Wheelbot: A testbed for learning-based balancing, flips, and articulated driving," in *Proc. IEEE Int. Conf. on Robotics and Automation (ICRA)*, 2025.

- [15] Y. Li, K. Hua, and Y. Cao, "Using stochastic programming to train neural network approximation of nonlinear MPC laws," *Automatica*, 2022.
- [16] C. M. Bishop, "Mixture density networks," 1994.
- [17] S. Lucia, D. Navarro, B. Karg, H. Sarnago, and O. Lucia, "Deep learning-based model predictive control for resonant power converters," *IEEE Trans. on Industrial Informatics*, vol. 17, no. 1, 2021.
- [18] A. Tulyan, B. Gopaluni, and P. Loewen, "A deep learning architecture for predictive control," *IFAC-PapersOnLine*, vol. 51, 01 2018.
- [19] M. Okamoto, J. Ren, Q. Mao, J. Liu, and Y. Cao, "Deep learning-based approximation of model predictive control laws using mixture networks," *IEEE Trans. on Autom. Science and Engineering*, 2024.
- [20] J. Carius, F. Farshidian, and M. Hutter, "MPC-Net: A first principles guided policy search," *IEEE Robotics and Automation Letters*, 2019.
- [21] P. Dhariwal and A. Nichol, "Diffusion models beat GANs on image synthesis," in *Advances in Neural Information Processing Systems*, vol. 34. Curran Associates, Inc., 2021, pp. 8780–8794.
- [22] A. Prasad, K. Lin, J. Wu, L. Zhou, and J. Bohg, "Consistency policy: Accelerated visuomotor policies via consistency distillation," in *Robotics: Science and Systems (RSS)*, 2024.
- [23] T.-Y. Huang, A. Lederer, N. Hoischen, J. Brüdigam, X. Xiao, S. Sosnowski, and S. Hirche, "Toward near-globally optimal nonlinear model predictive control via diffusion models," *arXiv:2412.08278*, 2024.
- [24] R. Römer, A. von Rohr, and A. P. Schoellig, "Diffusion predictive control with constraints," *arXiv preprint arXiv:2412.09342*, 2024.
- [25] A. Li, Z. Ding, A. B. Dieng, and R. Beeson, "Diffusolve: Diffusion-based solver for non-convex trajectory optimization," *arXiv preprint arXiv:2403.05571*, 2024.
- [26] J. Spencer, S. Choudhury, A. Venkatraman, B. Ziebart, and J. A. Bagnell, "Feedback in imitation learning: The three regimes of covariate shift," *arXiv:2102.02872*, 2021.
- [27] J. Ho, A. Jain, and P. Abbeel, "Denoising diffusion probabilistic models," in *Advances in Neural Information Processing Systems*, vol. 33, 2020, pp. 6840–6851.
- [28] P. Vincent, "A connection between score matching and denoising autoencoders," *Neural Computation*, vol. 23, pp. 1661–1674, 2011.
- [29] D. Limon, A. Ferramosca, I. Alvarado, and T. Alamo, "Nonlinear MPC for tracking piece-wise constant reference signals," *IEEE Trans. on Automatic Control*, vol. 63, no. 11, pp. 3735–3750, 2018.
- [30] J. Köhler, M. A. Müller, and F. Allgöwer, "A nonlinear tracking model predictive control scheme for dynamic target signals," *Automatica*, vol. 118, no. 109030, 2020.
- [31] A. Wächter and L. Biegler, "On the implementation of an interior-point filter line-search algorithm for large-scale nonlinear programming," *Mathematical Programming*, vol. 106, pp. 25–57, 03 2006.
- [32] M. Mittal, C. Yu, Q. Yu, J. Liu, N. Rudin, D. Hoeller, J. L. Yuan, R. Singh, Y. Guo, H. Mazhar, A. Mandlekar, B. Babich, G. State, M. Hutter, and A. Garg, "Orbit: A unified simulation framework for interactive robot learning environments," *IEEE Robotics and Automation Letters*, vol. 8, no. 6, pp. 3740–3747, 2023.
- [33] J. A. E. Andersson, J. Gillis, G. Horn, J. B. Rawlings, and M. Diehl, "CasADi – A software framework for nonlinear optimization and optimal control," *Mathematical Programming Computation*, 2019.
- [34] J. Carpentier, G. Saurel, G. Buondonno, J. Mirabel, F. Lamiraux, O. Stasse, and N. Mansard, "The Pinocchio C++ library – a fast and flexible implementation of rigid body dynamics algorithms and their analytical derivatives," in *IEEE Int. Symp. on System Integration*, 2019.
- [35] Y. Zhou, C. Barnes, J. Lu, J. Yang, and H. Li, "On the continuity of rotation representations in neural networks," in *IEEE/CVF Conference on Computer Vision and Pattern Recognition (CVPR)*, 2019.
- [36] A. Q. Nichol and P. Dhariwal, "Improved denoising diffusion probabilistic models," in *Proc. Int. Conf. on Machine Learning (ICML)*, vol. 139. PMLR, 2021, pp. 8162–8171.
- [37] S. Lin, B. Liu, J. Li, and X. Yang, "Common diffusion noise schedules and sample steps are flawed," in *Proceedings of the IEEE/CVF Winter Conference on Applications of Computer Vision*, 2024, pp. 5404–5411.
- [38] T. Hang, S. Gu, C. Li, J. Bao, D. Chen, H. Hu, X. Geng, and B. Guo, "Efficient diffusion training via Min-SNR weighting strategy," in *IEEE/CVF Int. Conf. on Computer Vision (ICCV)*, 2023.
- [39] D. Kappler, F. Meier, J. Issac, J. Mainprice, C. G. Cifuentes, M. Wüthrich, V. Berenz, S. Schaal, N. Ratliff, and J. Bohg, "Real-time perception meets reactive motion generation," *IEEE Robotics and Automation Letters*, vol. 3, no. 3, pp. 1864–1871, 2018.
- [40] J. Song, C. Meng, and S. Ermon, "Denoising diffusion implicit models," in *Int. Conf. on Learning Representations (ICLR)*, 2021.